Eur. Phys. J. D (2024)78:103
https://doi.org/10.1140/epjd/s10053-024-00890-y

THE EUROPEAN PHYSICAL JOURNAL D

Regular Article - Ultraintense and Ultrashort Laser Fields

Spectral phase pulse shaping reduces ground state depletion in high-order harmonic generation

J. Aygun[1], C. G. Buitrago[2,3,4], M. F. Ciappina[2,3,4], and A. L. Harris[1,a]

[1] Department of Physics, Illinois State University, Normal, IL, USA
[2] Department of Physics, Guangdong Technion - Israel Institute of Technology, 241 Daxue Road, Shantou 515063, Guangdong, China
[3] Technion - Israel Institute of Technology, 32000 Haifa, Israel
[4] Guangdong Provincial Key Laboratory of Materials and Technologies for Energy Conversion, Guangdong Technion - Israel Institute of Technology, 241 Daxue Road, Shantou 515063, Guangdong, China

Received 18 March 2024 / Accepted 24 June 2024

Abstract. High-order harmonic generation (HHG) has become an indispensable process for generating attosecond pulse trains and single attosecond pulses used in the observation of nuclear and electronic motion. As such, improved control of the HHG process is desirable, and one such possibility for this control is through the use of structured laser pulses. We present numerical results from solving the one-dimensional time-dependent Schrödinger equation for HHG from hydrogen using Airy and Gaussian pulses that differ only in their spectral phase. Airy pulses have identical power spectra to Gaussian pulses, but different spectral phases and temporal envelopes. We show that the use of Airy pulses results in less ground state depletion compared to the Gaussian pulse, while maintaining harmonic yield and cutoff. Our results demonstrate that Airy pulses with higher intensity can produce similar HHG spectra to lower intensity Gaussian pulses without depleting the ground state. The different temporal envelopes of the Gaussian and Airy pulses lead to changes in the dynamics of the HHG process, altering the time-dependence of the ground state population and the emission times of the high harmonics.

1 Introduction

High-order harmonic generation (HHG) is an important process in attosecond physics, used to generate attosecond pulse trains [1] and single attosecond pulses [2], and study the temporal dynamics of electronic motion [3–5]. Complementary to free electron laser facilities, HHG offers an approach to generating XUV light that is accessible for table-top experiments. Improved control of the HHG process through increased intensity, harmonic selectivity, extended harmonic generation beyond the classical cutoff energy, and less reduction in ground state population are all desirable improvements. In particular, the depletion of ground state atoms plays a critical role in suppressing HHG in atoms [6–8]. At high laser intensities, a significant fraction of the atoms is ionized, depleting the ground state population available for ionization and subsequent recombination, which are essential steps in the HHG process. This reduction in ground state atoms leads to fewer electron re-collisions with parent ions, thereby decreasing the efficiency of high harmonic emission. Furthermore, high levels of ionization can lead to plasma formation, which disturbs electron trajectories and further reduces HHG efficiency by disrupting phase-matching [6]. Additionally, when laser pulses are not sufficiently short, the ground state is largely depleted before the pulse peak is reached [7]. Consequently, the HHG radiation is generated by electric fields lower than the pulse peak. Airy pulses offer an opportunity to efficiently overcome these scenarios.

Different approaches have been undertaken in order to address some of the challenges associated with HHG, including using non-gas-phase targets [9–11], using structured laser fields [12, 13], controlling the pulse chirp [14], and controlling electron trajectories [12]. In the case of non-gas phase targets, nanostructures have been used to enhance the effects of the applied laser field [10, 15, 16]. This allowed for a lower intensity pulse to be used to produce the high harmonics. Additionally, with nanostructure targets, the nonhomogeneous electric field can lead to the production of even harmonics [9]. Initial practical challenges to these approaches have been overcome through the use of 3D wave guides that are less affected by thermal or optical damage and can create HHG with high spatiotemporal coherence [10, 15]. However, the efficiency of these techniques can still

[a] e-mail: alharri@ilstu.edu (corresponding author)

Published online: 13 August 2024

be improved, as the desired high repetition rates in the MHz range remain challenging [17].

Structured pulses are often generated with two-color laser fields [18–20], consisting of the fundamental field and one of its harmonics. The shape of the pulse envelope is altered by changing the relative phase between the two components. HHG with two-color fields has shown an enhancement in both yield and cutoff energy [11, 12, 21], as well as the ability to control photon energy, spectral properties, temporal dynamics, and polarization [20, 22, 23]. Additional methods to sculpt the laser field or control the HHG spectrum include temporally-delayed pulses [24], frequency mixing [25, 26], and combined static and laser fields [27–29]. These techniques have shown the ability to narrow harmonics [24], simplify experimental setups [24], increase yields [24, 29], and create a second plateau [28].

Here, we present theoretical calculations of the HHG spectrum and time-dependent ground state populations using an alternative means to control the temporal structure of the pulse through alteration of the pulse's spectral phase. Specifically, we examine third-order spectral phase effects using Airy pulses. The Airy pulses are chosen such that the power spectrum is identical to that of a Gaussian pulse, which allows for the direct comparison of pulses with identical power spectra, but different spectral phases and temporal envelopes.

The HHG process is frequently described using a classical 3-step model. In step 1, an electron is ionized from the target. In step 2, the electron moves classically in the electric field of the laser and then recombines with the residual ion to produce harmonics in step 3. Recent simulations of above threshold ionization [30] showed that the use of an Airy laser pulse altered the number and timing of ionization events relative to a Gaussian pulse and that the Airy pulse changed the photoelectron's energy and momentum. Because of the similarities of the first two steps of the HHG and ATI processes, the results of [30] suggest that laser pulses sculpted through the spectral phase may result in changes to the HHG spectrum. For example, a change in the ionization times could alter the kinetic energy of the recombining electron, which in turn could affect the HHG cutoff energy. Additionally, a change in the number of ionization events could alter the HHG yield.

We perform calculations using the time-dependent Schrödinger equation for HHG production from hydrogen. Our results show that Airy pulses with third-order spectral phases that have a nearly Gaussian envelope result in less depletion of the ground state population while maintaining harmonic cutoff and yield. We demonstrate that by controlling the third-order phase of the Airy pulse, it is possible to use higher intensity pulses without further depleting the ground state population. Additionally, the use of an Airy pulse alters the temporal dynamics of the ground state population and the timing of the harmonic production.

The remainder of the paper is organized as follows. Section 2 contains the theoretical and numerical methods used. Section 3 presents the results and Section 4 provides a brief summary and discussion. Atomic units are used throughout unless otherwise noted.

2 Time-dependent Schrödinger equation theory

The main qualitative features of HHG with linearly polarized pulses happen along the laser polarization direction, and therefore, a one-dimensional approximation is sufficient to capture the important physics. In particular, when the driving laser field is linearly polarized, the electron dynamics primarily occur in the same direction. However, a one-dimensional model cannot capture the effects due to the electron wave packet's initial transverse momentum, which are known to affect the HHG efficiency during acceleration in the laser continuum and recombination. We have chosen a one-dimensional model potential [31] that has been shown to reasonably approximate a three-dimensional model, but any direct comparison must be done with care. Because the main purpose of this study is to compare HHG spectra and ground state populations for different types of driving pulses, a one-dimensional model is suitable for this study [32].

The one-dimensional TDSE for a single active electron atom in a linearly polarized laser field is given in the dipole approximation and length gauge by

$$i\frac{\partial}{\partial t}\psi(x,\,t) = \left[-\frac{1}{2}\frac{\mathrm{d}^2}{\mathrm{d}x^2} + V_{\mathrm{a}}(x) + xE(t)\right]\psi(x,\,t), \tag{1}$$

where $V_{\mathrm{a}}(x)$ is the atomic potential and $E(t)$ is the laser pulse electric field. Several model potentials are available in the literature that are able to produce results that reasonably approximate those of full three-dimensional calculations [31, 33, 34]. We use the pliant core model [31]

$$V_{\mathrm{a}}(x) = -\frac{1}{(|x|^{\alpha} + \beta)^{\frac{1}{\alpha}}}, \tag{2}$$

because it has a sharp cusp feature at the origin and has been shown to reasonably approximate the magnitude and plateau cutoff values of 3-dimensional HHG and above threshold ionization calculations [31, 33]. The pliant core model parameters for hydrogen are $\alpha = 1.5$ and $\beta = 1.45$, which yield an ionization potential of 13.6 eV.

The TDSE was solved using the Crank–Nicolson method [35] and the initial state atomic wave function was found by imaginary time propagation. To prevent reflections from the spatial grid boundary, absorbing boundary conditions [36] were used and the density of the wave function was checked at each time step to ensure that no probability was lost. The spatial grid spanned from − 3000 to 3000 a.u. with a stepize of 0.07 a.u. A temporal stepsize of 0.01 a.u. was used.

The Fourier transform of the dipole acceleration was used to calculate the harmonic yield [37]

$$I_{\mathrm{HHG}} = |a_{\mathrm{d}}(\omega)|^2, \tag{3}$$

where

$$a_{\mathrm{d}}(\omega) = \int_{-\infty}^{\infty} \mathrm{d}t' a_{\mathrm{d}}(t') e^{i\omega t'} \tag{4}$$

and

$$\langle a_{\mathrm{d}}(t)\rangle = \langle \psi(t)|\frac{\partial V_{\mathrm{a}}(x)}{\partial x} + E(x,\, t)|\psi(t)\rangle. \tag{5}$$

The total ionization probability can be found from.

$$P_{\mathrm{ion}} = 1 - \sum_n P_n, \tag{6}$$

where the population P_n of a given bound state $\varphi_n(x)$ was found by projecting the final state wave function onto the bound state.

$$P_n = |\langle \varphi_n(x)|\psi(x,\, t_f)\rangle|^2. \tag{7}$$

The principle quantum number of the bound state is n and 7 states were included in our calculation of the total ionization probability.

Time–frequency analysis was performed to estimate the emission times of the harmonics using the Gabor transform [38]

$$a_{\mathrm{G}}(\omega,\, t) = \int \mathrm{d}t' a_{\mathrm{d}}(t') \frac{\exp\left[-\frac{(t'-t)^2}{2\sigma^2}\right]}{\sigma\sqrt{2\pi}} \exp(i\omega t'), \tag{8}$$

where σ is chosen as $\frac{1}{3\omega_{\mathrm{L}}}$ with the central laser frequency of the pulse given by ω_{L}.

The laser pulse has either a Gaussian or Airy envelope. The Gaussian pulse is given by

$$E_{\mathrm{G}}(t) = E_0 e^{-2\ln 2\left(\frac{t-t_{\mathrm{c}}}{\Delta t}\right)^2} \sin(\omega_0(t-t_{\mathrm{c}})) \tag{9}$$

, and the Airy pulse is given by [39]

$$E_{\mathrm{A}}(t) = E_0\sqrt{\frac{\pi}{2\ln 2}}\frac{\Delta t}{\tau_0} \times Ai\left(\frac{\tau-(t-t_{\mathrm{c}})}{\Delta\tau}\right) e^{\frac{\ln 2\left(\frac{2\tau}{3}-(t-t_{\mathrm{c}})\right)}{2\tau_{1/2}}} \sin(\omega_0(t-t_{\mathrm{c}})), \tag{10}$$

where ω_0 is the carrier frequency, Δt is the full width half maximum of the temporal intensity, $\Delta\tau$ is the stretch of the Airy, $\tau_{1/2}$ is the exponential truncation half-life of the Airy, τ is the shift of the Airy, t_{c} is the center of the pulse, and $\tau_0 = \left(\frac{|\phi_3|}{2}\right)^{1/3}$ is a parameter related to the third-order term ϕ_3 of the spectral phase. For the Airy pulse, the shape of the temporal envelope is controlled by the third-order spectral phase ϕ_3 (see Fig. 1), which is related to the truncation half-life, stretch, and shift of the Airy by

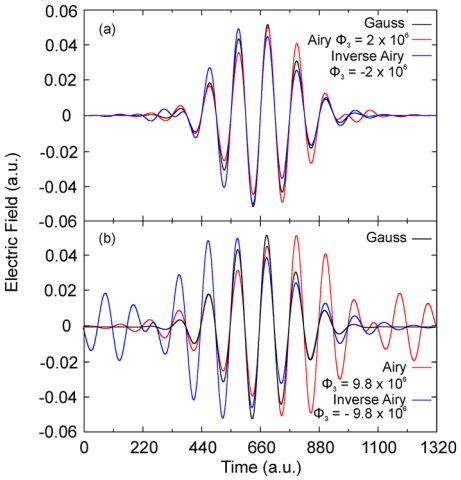

Fig. 1 Electric fields for 800 nm pulses used in the simulations with $\Delta t = 220$ a.u. **a** The intensity is $I = 1 \times 10^{14}\mathrm{W/cm^2}$. **b** The intensity is $I = 1 \times 10^{14}\mathrm{W/cm^2}$ for the Gaussian pulse and $I = 1.5 \times 10^{14}\mathrm{W/cm^2}$ for the Airy and inverse Airy pulses. Values of ϕ_3 are given in a.u

$$\tau_{1/2} = \frac{2(\ln 2)^2\phi_3}{\Delta t^2} \tag{11}$$

$$\Delta\tau = \tau_0 \mathrm{sign}(\phi_3) \tag{12}$$

$$\tau = \frac{\Delta t^4}{32(\ln 2)^2\phi_3}. \tag{13}$$

Figure 1 shows the electric fields as a function of time for the Gaussian and Airy pulses used in the simulations. The maximum electric field can be found from the laser intensity through $I = \frac{1}{2}\epsilon_0 cE^2$. Airy pulses with smaller magnitudes of the third-order spectral phase more closely resemble the Gaussian pulse, while larger values of the third-order spectral phase result in temporal pulse shapes that are very different from a Gaussian. For large values of $|\phi_3|$, side lobes appear in the temporal pulse envelope and the total width of the pulse increases. A negative ϕ_3 value reflects the pulse about its center, and we refer to these pulses as inverted Airy pulses. The pulses used in the simulations were truncated to 12 cycles (1320 a.u.) and the HHG spectrum was calculated at the end of the pulse. 12-cycle pulses allowed for inclusion of two lobes in the Airy pulses with the largest $|\phi_3|$ values used here. For both the Gaussian and Airy pulses, keeping more than 12 cycles had no effect on the HHG spectrum or the ground state population, indicating that the additional lobes of the

Airy pulse have no detectable influence on ionization or harmonic production.

One of the features of the Gaussian and Airy pulses is that their spectral intensities are identical, and the frequency domain electric fields differ only by the third-order phase. For the Gaussian pulse, the frequency domain electric field is

$$E_{\mathrm{G}}(\omega) = \frac{E_0 \Delta t \sqrt{\pi}}{2^{3/2}\sqrt{\ln 2}} e^{-\frac{\Delta t^2(\omega_0-\omega)^2}{(8\ln 2)}} \tag{14}$$

and for the Airy pulse, the frequency domain electric field is [39]

$$E_{\mathrm{A}}(\omega) = E_{\mathrm{G}}(\omega) e^{-\frac{i}{6}\phi_3(\omega-\omega_0)^3}. \tag{15}$$

3 Results

During the HHG process, as the laser pulse ionizes the atomic target, the proportion of atoms in the ground state is reduced. While some of the ionized electrons recombine with the parent ion to produce the high harmonics, many are either rescattered or driven away from the ion causing a lasting depletion of the ground state population. Significant depletion can result in reduced efficiency of the HHG process. In general, an increased laser intensity will result in an increased ionization rate and a corresponding increase in ground state depletion. Thus, a mechanism to limit ground state depletion while increasing laser intensity and maintaining or enhancing HHG efficiency is desirable. We demonstrate that Airy pulses provide a means of temporal envelope shaping through control of the pulse's spectral phase, which results in a smaller ground state depletion than other pulses at the same intensity.

Figure 2a shows the ground state population as a function of time for Gaussian and Airy pulses with identical intensities ($I = 1 \times 10^{14}$ W/cm^2). Despite nearly identical electric fields (top of Fig. 2a), the dynamics of the ground state populations are different. The inverted Airy pulse causes a drop in ground state population earlier than the Gaussian pulse, while the Airy pulse causes a delayed decrease in ground state population. Both the Airy and inverted Airy pulses lead to the same final ground state population, which is 4.5% higher than that of the Gaussian pulse (0.91 vs. 0.87). However, this enhanced final ground state population does not result in an increased harmonic yield, possibly due to the reduced ionization probability of the Airy pulses (Fig. 3). Fewer ionization events result in fewer electrons available for recombination and harmonic production.

The HHG spectra of the Gaussian and Airy pulses from Fig. 2a are shown in Fig. 2b–d. The harmonic yield for all pulses is nearly identical, although there is a very slight decrease in the HHG plateau cutoff for the

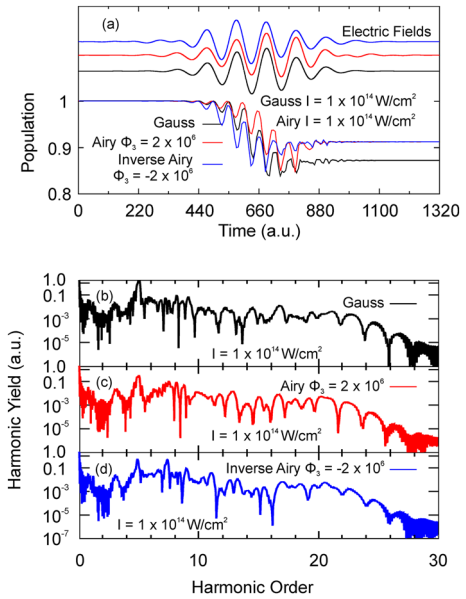

Fig. 2 **a** Electric fields (top) and time-dependent ground state populations (bottom) for HHG of hydrogen using 12 cycle, 800 nm Gaussian (black line), Airy (red line), and inverted Airy (blue line) pulses. The intensity of the laser pulses was 1×10^{14}W/cm^2. The third-order phase for the Airy and inverted Airy pulses was 2×10^6a.u. and -2×10^6a.u., respectively. **b**–**d** HHG spectra for the same laser pulses as (**a**)

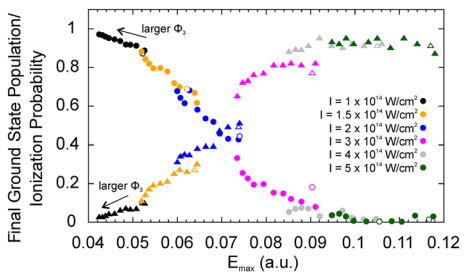

Fig. 3 Final ground state population (circles) and ionization probability (triangles) at end of the pulse for Gaussian (open circles/triangles) and Airy pulses (filled circles/triangles). The different colors of data correspond to different laser intensities as denoted in the figure. For a given laser intensity, the data points correspond to different third-order phases with the left-most data point for each intensity corresponding to an Airy pulse with the largest third-order phase ($|\phi_3| = 10^7$a.u.)

Airy pulses relative to the Gaussian pulse. The harmonics produced in the HHG process are a direct indication of the photoelectron's energy at the time of recollision, which results from the energy gained during its time in the laser field. Within the classical 3-step model, the electron is assumed to tunnel out of the atomic barrier at the origin with zero initial velocity. During its time in the laser field, it gains a maximum kinetic energy of 3.17 U_{p} + I_{p}, where U_{p} is the Pondermotive energy and I_{p} is the ionization potential. The Pondermotive

energy is defined as the cycle-averaged kinetic energy [40], and for long pulses, is directly proportional to the intensity and the square of the fundamental wavelength of the laser field. Thus, the classically predicted HHG plateau cutoff occurs at this maximum energy. However, for short pulses, the field intensity is different for each optical cycle, and an important consideration is the variation in the Pondermotive energy with pulse cycle [40]. This cycle-dependent variation in Pondermotive energy can cause the HHG plateau cutoff to differ from the classically predicted value. Additionally, within a quantum orbit model, the predicted cutoff value is larger than the classically predicted one [41], introducing another possible shift of the HHG plateau cutoff value.

In Fig. 2, the last harmonic occurs around the 27th harmonic with an intensity more than an order of magnitude smaller than harmonics in the plateau region, which ends at the 23rd harmonic. This last harmonic occurs at a larger energy than the classically predicted cutoff at the 21st harmonic or the quantum orbit predicted cutoff at the 24th harmonic. However, the end of the HHG plateau occurs at an energy between the classical and quantum orbit predicted cutoffs. It is not uncommon for the plateau cutoff to vary slightly from the classical or quantum orbit predicted values [9], especially considering the effects of pulse duration and envelope shape discussed above.

When comparing the Airy and Gaussian pulses used in these calculations (Fig. 1a), the maximum intensities of the electric fields are nearly identical at the center of the pulse and will result in nearly identical initial kinetic energies of the photoelectrons for this cycle of the pulse. However, the Airy pulses exhibit a slight temporal asymmetry due to their asymmetric envelope. This asymmetry alters the strength of the Airy electric field relative to the Gaussian electric field for cycles away from the pulse's center, which in turn would alter the electron's kinetic energy. If significant, this change in the kinetic energy would result in a change in the HHG spectrum, including the cutoff energy. However, the similarity of the HHG spectra in Fig. 2b–d indicates that any change to the electron's kinetic energy caused by the Airy pulse asymmetry is not significant enough to alter the HHG spectrum for values of $|\phi_3|$ that give a pulse with a near-Gaussian envelope. In general, the similarities of the spectra in Fig. 2b–d, combined with the ground state population dynamics of Fig. 2a, indicate that less depletion of the ground state population can be achieved using Airy pulses with near-Gaussian envelopes while maintaining harmonic yield and plateau cutoff. This feature provides a possible means of ground state population control.

The carrier envelope phase (CEP) of the pulse is defined as the offset of the maximum of the electric field (carrier wave) relative to the maximum of the pulse envelope. In the HHG process, the CEP is known to play an important role in the harmonic spectrum [42, 43]. Within the 3-step model, a change in the CEP can alter the release time of the electron relative to the pulse envelope, causing a change in the magnitude of the vector potential experienced by the tunneled electron and thus a change in its recollision energy. Here, we have chosen a laser pulse such that the electric field at the temporal center of the pulse is zero. For Gaussian pulses, this causes the maximum of the laser field to not occur at the maximum of the pulse envelope, and results in a CEP of $\pi/4$ for the Gaussian pulse. However, for Airy pulses, the envelope shape is asymmetric, and the maximum of the envelope does not occur at the temporal center. This changes the carrier envelope phase of the Airy pulse relative to the Gaussian pulse, despite the fact that the electric field of both pulses is zero at the temporal center of the pulse. For the Airy and inverted Airy pulses of Figs. 1a and 2, the CEP was $-\pi/5.6$, and $\pi/5.6$, respectively. For the Airy and inverted Airy pulses of Figs. 1b and 6 it was $\pi/14.5$ and $-\pi/14.5$, respectively.

As the Airy third-order phase increases, the pulse envelope becomes less Gaussian and the maximum electric field of the pulse decreases, despite a constant intensity. This decrease in the maximum electric field strength results in a decreased high harmonic plateau cutoff (not shown) and an increase in the final ground state population at the end of the laser pulse. Figure 3 shows the final ground state population (circles) and final ionization probability [triangles; calculated from Eq. (6)] for Gaussian and Airy pulses with different third-order phase terms ($|\phi_3| = 1, 1.5, 2, 3, \ldots, 10 \times 10^6$ a.u.). Open circles/triangles are data for Gaussian pulses and the left-most data point for each color results from Airy pulses with the largest third-order phase value of the simulations ($|\phi_3| = 10^7$ a.u.). The sign of the third-order phase term causes different temporal dynamics of the ground state population, as shown in Fig. 2a, but the final ground state population and the ionization probability are independent of the sign of the third-order phase term. Data points of the same color result from pulses with the same intensity and results for six different intensities are shown. Note that intensities below 3×10^{14} W/cm^2 are below the saturation threshold for hydrogen [44], and thus the target atoms are expected to be fully ionized for pulses at or above this intensity.

Figure 3 shows that for a given intensity, as the magnitude of the phase increases, the final ground state population is larger and the total ionization probability is reduced. This implies that Airy pulses with larger $|\phi_3|$ values result in fewer ionization events, which results in a larger ground state population. However, Fig. 2 shows that the harmonic yield for Airy pulses with smaller $|\phi_3|$ values is nearly identical to that of the Gaussian pulse. In order to maintain the harmonic yield with fewer ionized electrons, the recombination rate must be increased and therefore the data in Figs. 2 and 3 indicate that electrons ionized by Airy pulses may have a higher recombination rate. Classical calculations [45] confirm that the number and timing of recombinations is different for Airy pulses compared to Gaussian pulses. Both the Airy and inverted Airy pulses cause more recombination events than the Gaussian pulse. Additionally, as $|\phi_3|$ increases, the maximum electric field decreases

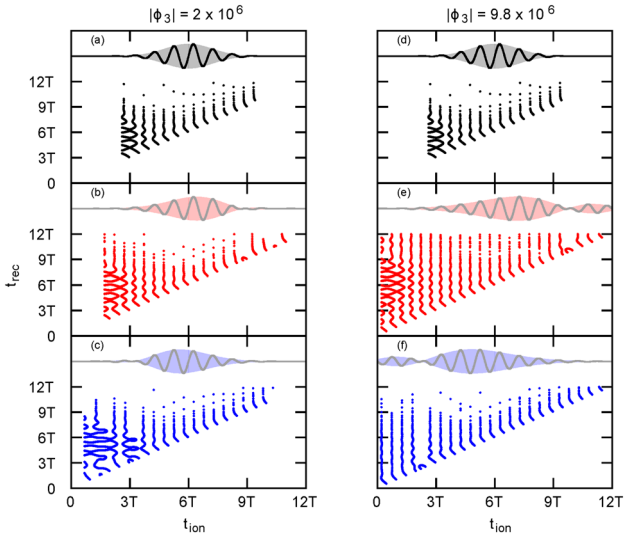

Fig. 4 Electron recombination times as a function of ionization time calculated using a classical model [45]. Times are shown in units of optical cycles. Each data point represents a possible recombination event. The electric fields are shown at the top of each panel. **a**, **d** Gaussian pulses. **b**, **e** Airy pulses. **c**, **f** inverted Airy pulses. The third-order spectral phases are listed at the top of each column for the Airy and inverted Airy pulses. **a**–**d** Intensity was 1×10^{14} W/cm^2. **e**,**f** Intensity was 1.5×10^{14} W/cm^2. The results in (**a**) and **d** are identical

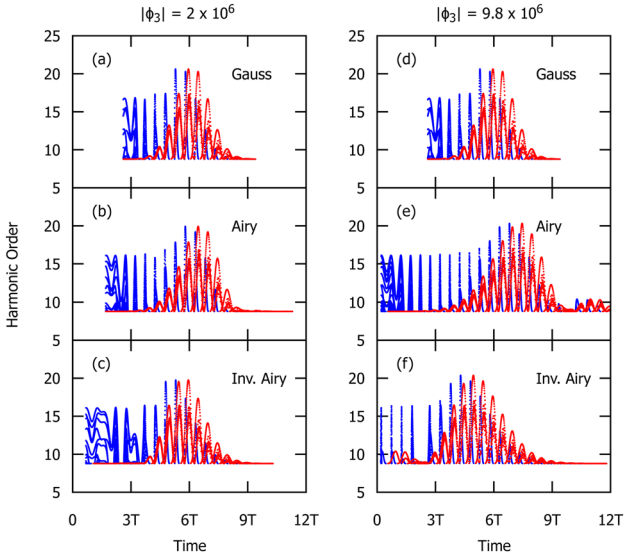

Fig. 5 Electron kinetic energies at the time of recombination (in units of the harmonic order) calculated using a classical model [45]. Each data point represents a recombination event. Energies are shown as a function of the ionization time (blue dots) or recombination time (red dots) with times given in optical cycles (T). The third-order spectral phases are listed at the top of each column for the Airy and inverted Airy pulses. **a**–**d** Intensity was 1×10^{14} W/cm^2. **e**,**f** Intensity was 1.5×10^{14} W/cm^2. The results in **a** and **d** are identical

with the exception of the smallest $|\phi_3|$ value used here ($|\phi_3| = 10^6$ a.u., right most data point of each color), in which the Airy maximum electric field is greater than the Gaussian maximum electric field.

Classical calculations that solve Newton's equation of motion for an electron in an oscillating electric field [45] can provide additional insight into the dynamics of the electrons after ionization. Figure 4 shows a plot of the possible recombination times as a function of ionization time for the three pulse types. A single point in the figure indicates a ($t_{\rm ion}$, $t_{\rm rec}$) pair and a higher value on the vertical axis indicates that the recombination occurred later after ionization. Because ionization is unlikely to occur when the pulse strength is negligible, we show only ($t_{\rm ion}$, $t_{\rm rec}$) pairs for when the electric field is greater than 1% of E_0. A vertical line drawn through the plot would indicate the number of possible recombination times for a given ionization time. As expected, in all cases, an electron ionized earlier in the pulse has more opportunities to recombine with the parent ion due to it experiencing more oscillations of the electric field that can drive it back to the parent ion.

Figure 4 shows that the different pulse shapes lead to different numbers of possible recombination times after ionization. For the Airy and inverted Airy pulses, there are more possible recombination times, due in part to the electric field being non-negligible for a longer time. This greater duration of the electric field causes electrons to be ionized at both earlier and later times compared to the Gaussian pulse leading to overall more possible recombination times.

Figure 5 shows the classical prediction for the kinetic energy spectrum of the recombining electrons as a function of the ionization time (blue dots) and recombination time (red dots). The kinetic energy spectrum is clearly affected by the laser pulse shape, particularly for large $|\phi_3|$. The spectra show that the highest kinetic energy predicted by the classical calculation corresponds to the 21st harmonic and that for $|\phi_3| = 2 \times 10^6$ a.u., electrons with this kinetic energy are produced at two ionization times for all of the pulse shapes. For $|\phi_3| = 9.8 \times 10^6$ a.u., the electrons corresponding to the 21st harmonic are produced at two ionization times for the Gaussian and Airy pulses, but only one ionization time for the inverted Airy pulse. The times for the production of the highest order harmonic vary with pulse envelope shape and occur near the maxima of the electric fields. Both the Airy and inverted Airy pulses produce electrons with kinetic energy greater than 15 harmonic orders earlier than the Gaussian pulse due to the extended duration of the pulses. For $|\phi_3| = 9.8 \times 10^6$ a.u., a gap is observed in the kinetic energy spectra that corresponds to the node in the envelope of the Airy and inverted Airy pulses.

The kinetic energy spectra as a function of recombination time provide a classical prediction of the timing of harmonic production. These spectra resemble the shape of the pulse envelopes and show a clear difference in harmonic production times for the different pulses.

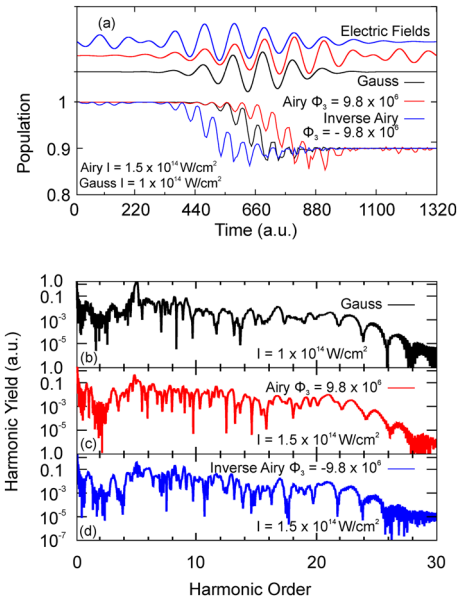

Fig. 6 **a** Electric fields (top) and time-dependent ground state populations (bottom) for HHG using Gaussian (black line), Airy (red line), and inverted Airy (blue line) pulses. The intensity of the laser pulses was 1×10^{14}W/cm^2 for the Gaussian pulse and 1.5×10^{14}W/cm^2 for the Airy and inverted Airy pulses. The third-order phase for the Airy and inverted Airy pulses was 9.8×10^6a.u. and -9.8×10^6a.u., respectively. **b**–**d** HHG spectra for the same laser pulses as (**a**)

For a Gaussian pulse, the harmonics are produced symmetrically about the pulse's temporal center. However, for the Airy pulse, the harmonics are produced after the temporal center, while for the inverted Airy pulse, they are produced before the temporal center. In the case of $|\phi_3| = 9.8 \times 10^6$ a.u., the secondary lobes of the Airy (inverted Airy) pulses result in the production of harmonics (order 11) at later (earlier) times that are not present for the Gaussian pulse.

In some cases, the same final ground state population and ionization probability can be achieved for different pulse intensities through control of the third-order phase. For example, a Gaussian pulse with $I = 1 \times 10^{14}$ W/cm^2 (black open circle, Fig. 3) and an Airy pulse with $|\phi_3| = 9.8 \times 10^6$ a.u. and $I = 1.5 \times 10^{14}$ W/cm^2 a.u. (yellow solid circle, Fig. 3) result in identical final ground state populations and ionization probabilities. This indicates that a more intense laser pulse can be applied without affecting the ground state population if a third-order phase is introduced.

Figure 6 shows the time-dependent ground state populations and the HHG spectra for the example above in which the final ground state populations and ionization rates are identical for different pulse types. In Fig. 6a, the inverted Airy pulse depletes the ground state much earlier than the Gaussian or Airy pulses, despite the final populations being identical. The timing of the depletion reflects the envelope of each pulse. Importantly, the increased intensity of the Airy pulse does not result in an increased ground state depletion and does not significantly alter the HHG yields or cutoffs (Fig. 6b–d). This indicates that the overall harmonic emission is not affected by the timing of ionization or the pulse shape.

To investigate the temporal dynamics of HHG production further, we show in Fig. 7 the Gabor transform [38, 46] of the dipole acceleration. These plots show the timing and intensity of harmonic production. Warmer colors indicate more intense production while taller peaks indicate production of higher order harmonics. In Fig. 7a–c, the intensities of the pulses are identical (same as Fig. 2), while in Fig. 7d–f, the intensities are different, but the pulses yield the same final ground state population (same as Fig. 6).

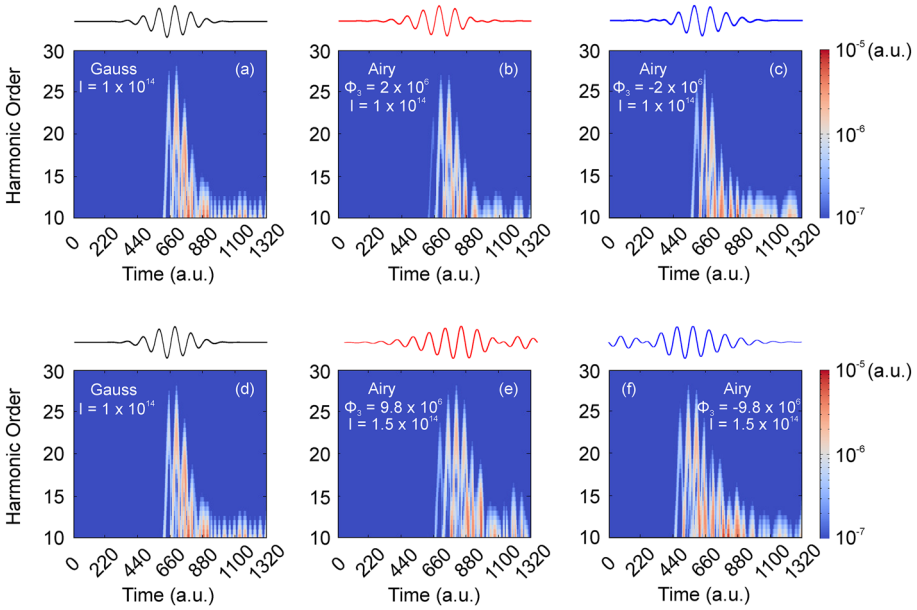

Fig. 7 Electric fields (top panel) and Gabor transform (bottom panel) showing time–frequency analysis for HHG with Gaussian and Airy pulses. **a**–**c** Laser intensity was $I = 1 \times 10^{14}$W/cm^2. **d**–**f** Laser intensity was $I = 1 \times 10^{14}$W/cm^2 for the Gaussian pulse and $I = 1.5 \times 10^{14}$W/cm^2 for the Airy pulses. Third-order phase values (in a.u.) are shown in the figure

Figures 7a–c show all three pulses produce harmonics up to order ~ 27 but the time at which the harmonics are produced varies with the pulse envelope shape. Similar trends are observed in Figs 7d–f, with all three pulses producing harmonics up to order ~ 27, but the effect of the pulse envelope shape is more pronounced. The Airy pulse produces harmonics of order 15–20 later in time (Fig. 7e), while the Gaussian and inverted Airy do not. Also, the inverted Airy pulse produces the highest order harmonics earlier in time ($t \approx 550$ a.u.) than the Gaussian ($t \approx 700$ a.u.) or Airy ($t \approx 800$ a.u.) pulses.

The results from the Gabor transforms, combined with our classical simulations, clearly indicate that the pulse's spectral phase (and subsequent temporal envelope shape) alters the time of ionization events and the time of high order harmonic production. The inverted Airy pulse causes earlier ionization events because the electric field is enhanced at earlier times relative to the Gaussian or Airy pulse. Consequently, the recombination time also occurs earlier in time. However, the similarity of the HHG spectra in Figs. 2 and 6 for the different pulse shapes signifies that the different timing of ionization and recombination events does not change the HHG yield or plateau cutoff. Thus, the number of photoelectrons produced, and their energy, are not affected by the timing of ionization and recombination.

4 Conclusion

High-order harmonic generation has become ubiquitous in attosecond physics, prompting significant efforts to improve efficiency of production, increase harmonic plateau cutoff, enhance harmonic selectivity, and control ground state depletion. Some of these efforts have focused on pulse shaping, primarily through the use of two-color fields. We presented calculations for HHG from hydrogen using an alternative technique for pulse shaping using the spectral phase of the laser pulse. We used the time-dependent Schrödinger equation to calculate the harmonic spectra and ground state populations for Airy and Gaussian laser pulses with the same spectral intensity but different spectral phases. The presence of the third-order spectral phase of the Airy pulse altered the temporal envelope of the electric field, leading to changes in the time-dependent ground state population and timing of ionization and harmonic production.

Our simulations demonstrated that an Airy pulse with the same intensity as a Gaussian pulse resulted in a reduced ground state depletion and a reduced ionization rate. These changes were counterbalanced by an increase in recombination events, resulting in nearly identical harmonic yields for the Gaussian and Airy pulses. Classical simulations confirmed that despite a reduced ionization rate, Airy pulses resulted in increased recombination events. Additionally, for values of the third-order phase that result in a near-Gaussian shaped envelope, the harmonic plateau cutoff was not significantly altered. Thus, Airy pulses with smaller third-order phases resulted in less ground state depletion without reducing the harmonic yield or cutoff. Importantly, we showed that the introduction of the third-order phase of the Airy pulse allowed for the use of a higher intensity laser pulse without reducing the ground state population. By controlling the third-order phase, in combination with the pulse intensity, it was possible to have Gaussian and Airy pulses with different intensities yield the same ground state population and ionization probability.

Because the spectral phase of the Airy pulse alters the temporal envelope of the electric field, the temporal dynamics of the HHG process were also altered. Our results showed that while Airy and inverted Airy pulses resulted in the same final ground state depletion at the end of the pulse, the ground state was depleted earlier for inverted Airy pulses and later for Airy pulses. This change in dynamics caused a change in the timing of the harmonic production. A Gabor analysis revealed that the same harmonics are produced for the different pulses, but at different times. The inverted Airy pulse produced harmonics earlier in time, while the Gaussian and Airy pulses produced harmonics later.

Overall, our results demonstrated that the spectral phase of the laser pulse can be used to control some features of the high-order harmonic process. The ability to use a more intense laser pulse while maintaining ground state population could open the door to the use of new or previously inaccessible targets. Additionally, control of the third-order phase can provide a method to control the timing of HHG production. The use of a laser pulse with a nonzero spectral phase provides an additional control parameter that can limit undesirable effects, like, for instance, the amount of ionization. Here, free electrons in the partially ionized gas medium are known to prevent phase matching and limit the upconversion efficiency. Therefore, any approach able to control them deserves consideration.

Acknowledgements A. L. H. and J. A. acknowledge the support of the National Science Foundation under Grant No. PHY-2207209 and the Illinois State University High Performance Computing resources. M. F. C. and C. G. acknowledge financial support by the Guangdong Province Science and Technology Major Project (Future functional materials under extreme conditions -2021B0301030005) and the Guangdong Natural Science Foundation (General Program project No. 2023A1515010871).

Author contributions

All authors contributed to the study conception and design. Calculations and analysis were performed by all authors. The first draft of the manuscript was written by A. L. Harris, and all authors commented on previous versions of the manuscript. All authors read and approved the final manuscript.

Data Availability Statement This manuscript has associated data in a data repository. [Authors' comment: The authors declare that the data supporting the findings of this study are available within the paper and FigShare (https://doi.org/10.6084/m9.figshare.25425613)].

References

1. P.M. Paul, E.S. Toma, P. Breger, G. Mullot, F. Augé, Ph. Balcou, H.G. Muller, P. Agostini, Observation of a train of attosecond pulses from high harmonic generation. Science **292**, 1689 (2001)
2. M. Hentschel, R. Kienberger, C. Spielmann, G.A. Reider, N. Milosevic, T. Brabec, P. Corkum, U. Heinzmann, M. Drescher, F. Krausz, Attosecond metrology. Nature **414**, 6863 (2001)
3. R. Kienberger et al., Steering attosecond electron wave packets with light. Science **297**, 1144 (2002)
4. M. Uiberacker et al., Attosecond real-time observation of electron tunnelling in atoms. Nature **446**, 7136 (2007)
5. K. Liu, Q. Zhang, P. Lu, Enhancing electron localization in molecular dissociation by two-color mid- and near-infrared laser fields. Phys. Rev. A **86**, 033410 (2012)
6. S. Varró, Quantum optical aspects of high-harmonic generation. Photonics **8**, 7 (2021)
7. X.-B. Bian, A.D. Bandrauk, Spectral shifts of nonadiabatic high-order harmonic generation. Appl. Sci. **3**, 1 (2013)
8. Kaertner, Franz X., *Ultrafast Optical Physics II* (Center for Free Electron Laser Science, n.d.).
9. M.F. Ciappina, J. Biegert, R. Quidant, M. Lewenstein, High-order-harmonic generation from inhomogeneous fields. Phys. Rev. A **85**, 033828 (2012)
10. S. Han, H. Kim, Y.W. Kim, Y.-J. Kim, S. Kim, I.-Y. Park, S.-W. Kim, High-harmonic generation by field enhanced femtosecond pulses in metal-sapphire nanostructure. Nat. Commun. **7**, 1 (2016)
11. F. Navarrete, U. Thumm, Two-color-driven enhanced high-order harmonic generation in solids. Phys. Rev. A **102**, 063123 (2020)
12. K.R. Hamilton, H.W. van der Hart, A.C. Brown, Pulse-shape control of two-color interference in high-order-harmonic generation. Phys. Rev. A **95**, 013408 (2017)
13. Y. Yang, R.E. Mainz, G.M. Rossi, F. Scheiba, M.A. Silva-Toledo, P.D. Keathley, G. Cirmi, F.X. Kärtner, Strong-field coherent control of isolated attosecond pulse generation. Nat. Commun. **12**, 1 (2021)
14. D.G. Lee, J.-H. Kim, K.-H. Hong, C.H. Nam, Coherent control of high-order harmonics with chirped femtosecond laser pulses. Phys. Rev. Lett. **87**, 243902 (2001)
15. I.-Y. Park, S. Kim, J. Choi, D.-H. Lee, Y.-J. Kim, M.F. Kling, M.I. Stockman, S.-W. Kim, Plasmonic generation of ultrashort extreme-ultraviolet light pulses. Nat. Photon **5**, 11 (2011)
16. N. Pfullmann et al., Bow-tie nano-antenna assisted generation of extreme ultraviolet radiation. New J. Phys. **15**, 093027 (2013)
17. M.F. Ciappina et al., Attosecond physics at the nanoscale. Rep. Prog. Phys. **80**, 054401 (2017)
18. K.J. Schafer, M.B. Gaarde, A. Heinrich, J. Biegert, U. Keller, Strong field quantum path control using attosecond pulse trains. Phys. Rev. Lett. **92**, 023003 (2004)
19. T.T. Liu, T. Kanai, T. Sekikawa, S. Watanabe, Significant enhancement of high-order harmonics below 10 nm in a two-color laser field. Phys. Rev. A **73**, 063823 (2006)
20. E. Mansten, J.M. Dahlström, P. Johnsson, M. Swoboda, A. L'Huillier, J. Mauritsson, Spectral shaping of attosecond pulses using two-colour laser fields. New J. Phys. **10**, 083041 (2008)
21. D. Peng, L.-W. Pi, M.V. Frolov, A.F. Starace, Enhancing high-order-harmonic generation by time delays between two-color, few-cycle pulses. Phys. Rev. A **95**, 033413 (2017)
22. J. Mauritsson, P. Johnsson, E. Gustafsson, A. L'Huillier, K.J. Schafer, M.B. Gaarde, Attosecond pulse trains generated using two color laser fields. Phys. Rev. Lett. **97**, 013001 (2006)
23. E.G. Neyra, F. Videla, D.A. Biasetti, M.F. Ciappina, L. Rebón, Twisting attosecond pulse trains by amplitude-polarization IR pulses. Phys. Rev. A **108**, 043102 (2023)
24. L. Gulyás Oldal, T. Csizmadia, P. Ye, N.G. Harshitha, A. Zair, S. Kahaly, K. Varjú, M. Füle, B. Major, Generation of high-order harmonics with tunable photon energy and spectral width using double pulses. Phys. Rev. A **102**, 013504 (2020)
25. H. Eichmann, S. Meyer, K. Riepl, C. Momma, B. Wellegehausen, Generation of short-pulse tunable XUV radiation by high-order frequency mixing. Phys. Rev. A **50**, R2834 (1994)
26. M.B. Gaarde, P. Antoine, A. Persson, B. Carré, A. L'Huillier, C.-G. Wahlström, High-order tunable sum and difference frequency mixing in the XUV region. J. Phys. B At. Mol. Opt. Phys. **29**, L163 (1996)
27. B. Wang, X. Li, P. Fu, The effects of a static electric field on high-order harmonic generation. J. Phys. B At. Mol. Opt. Phys. **31**, 1961 (1998)
28. S. Odžak, D.B. Milošević, High-order harmonic generation in the presence of a static electric field. Phys. Rev. A **72**, 033407 (2005)
29. M.-Q. Bao, A.F. Starace, Static-electric-field effects on high harmonic generation. Phys. Rev. A **53**, R3723 (1996)
30. A.L. Harris, Spectral phase effects in above threshold ionization. J. Phys. B At. Mol. Opt. Phys. **56**, 095601 (2023)
31. A.A. Silaev, MYu. Ryabikin, N.V. Vvedenskii, Strong-field phenomena caused by ultrashort laser pulses:

effective one- and two-dimensional quantum-mechanical descriptions. Phys. Rev. A **82**, 033416 (2010)
32. M. Protopapas, C.H. Keitel, P.L. Knight, Atomic physics with super-high intensity lasers. Rep. Prog. Phys. **60**, 389 (1997)
33. Y.-Y. Tian, S.-Y. Li, S.-S. Wei, F.-M. Guo, S.-L. Zeng, J.-G. Chen, Y.-J. Yang, Investigation on the influence of atomic potentials on the above threshold ionization. Chin. Phys. B **23**, 053202 (2014)
34. S. Majorosi, M.G. Benedict, A. Czirják, Improved One-dimensional model potentials for strong-field simulations. Phys. Rev. A **98**, 023401 (2018)
35. W.H. Press, W.T. Vettering, S.A. Teukolsky, B.P. Flannery, *Numerical Recipes in Fortran*, 2nd edn. (Cambridge University Press, Cambridge, 1992)
36. J.L. Krause, K.J. Schafer, K.C. Kulander, Calculation of photoemission from atoms subject to intense laser fields. Phys. Rev. A **45**, 4998 (1992)
37. A. Chacón, M.F. Ciappina, M. Lewenstein, Numerical studies of light-matter interaction driven by plasmonic fields: the velocity gauge. Phys. Rev. A **92**, 063834 (2015)
38. C.C. Chirilă, I. Dreissigacker, E.V. van der Zwan, M. Lein, Emission times in high-order harmonic generation. Phys. Rev. A **81**, 033412 (2010)
39. M. Wollenhaupt, A. Assion, T. Baumert, Femtosecond laser pulses: linear properties, manipulation, generation and measurement, in *Springer Handbook of Lasers and Optics*. ed. by F. Träger (Springer New York, New York, 2007), pp.937–983
40. R. Della Picca, A.A. Gramajo, C.R. Garibotti, S.D. López, D.G. Arbó, Nonconstant ponderomotive energy in above-threshold ionization by intense short laser pulses. Phys. Rev. A **93**, 023419 (2016)
41. M. Lewenstein, Ph. Balcou, MYu. Ivanov, A. L'Huillier, P.B. Corkum, Theory of high-harmonic generation by low-frequency laser fields. Phys. Rev. A **49**, 2117 (1994)
42. A. de Bohan, P. Antoine, D.B. Milošević, B. Piraux, Phase-dependent harmonic emission with ultrashort laser pulses. Phys. Rev. Lett. **81**, 1837 (1998)
43. M. Nisoli, G. Sansone, S. Stagira, S. De Silvestri, C. Vozzi, M. Pascolini, L. Poletto, P. Villoresi, G. Tondello, Effects of carrier-envelope phase differences of few-optical-cycle light pulses in single-shot high-order-harmonic spectra. Phys. Rev. Lett. **91**, 213905 (2003)
44. J.A. Pérez-Hernández, D.J. Hoffmann, A. Zaïr, L.E. Chipperfield, L. Plaja, C. Ruiz, J.P. Marangos, L. Roso, Extension of the cut-off in high-harmonic generation using two delayed pulses of the same colour. J. Phys. B At. Mol. Opt. Phys. **42**, 134004 (2009)
45. M.F. Ciappina, J.A. Pérez-Hernández, M. Lewenstein, ClassSTRONG: classical simulations of strong field processes. Comput. Phys. Commun. **185**, 398 (2014)
46. D. Gabor, Theory of communication. Part 1: the analysis of information. J. Inst. Electr. Eng. Part III Radio Commun. Eng. **93**, 429 (1946)